Available online at www.sciencedirect.com
SCIENCE DIRECT
Physica C 434 (2006) 53–61
PHYSICA C
www.elsevier.com/locate/physc

Distortion of ReO_6 octahedron in the $Hg_{0.82}Re_{0.18}Ba_2Ca_2Cu_3O_{8+d}$ superconductor

M.T.D. Orlando [a,*], C.A.C. Passos [a], J.L. Passamai Jr. [a], E.F. Medeiros [a], C.G.P. Orlando [a], R.V. Sampaio [a], H.S.P. Correa [b], F.C.L. de Melo [c], L.G. Martinez [d], J.L. Rossi [d]

[a] *Preslab—High Pressure Laboratory, UFES, Vitoria, ES 29075-910, Brazil*
[b] *Departamento de Física, Universidade Federal do Mato Grosso do Sul, Brazil*
[c] *Centro Técnico Aeroespacial—IAE, São José dos Campos-SP, CEP 12228-904, Brazil*
[d] *Instituto de Pesquisas Energéticas e Nucleares, Campus USP, Brazil*

Received 30 September 2005; accepted 30 November 2005
Available online 10 January 2006

Abstract

Rhenium (Re) L_{III} edge X-ray absorption spectroscopy was used in order to determine rhenium valence and the local oxygen coordination in $Hg_{0.82}Re_{0.18}Ba_2Ca_2Cu_3O_{8+d}$ polycrystalline samples prepared with three different oxygen content. Thermoelectric power measurements confirmed small increments of charge carrier number as a function of oxygen content. The X-ray absorption near-edge spectroscopy (XANES) analysis showed a valence variation for Re (+6.8, +6.9 and +7.0) in these samples. The extended X-ray absorption fine structure (EXAFS) analysis indicated that the oxygen local order around Re atoms in these $Hg_{0.82}Re_{0.18}Ba_2Ca_2Cu_3O_{8+d}$ samples can be described as a distorted ReO_6 octahedron with two different Re–O bound lengths. The valence evaluated by the bound length in the distorted ReO_6 octahedron is in agreement with the XANES measurements. Moreover, the distorted ReO_6 octahedron and the $Cu–O_{pl}$ angle built a scenario which can justify the high intrinsic term value found in the optimal doped sample under external hydrostatic pressure.

Keywords: XANES; EXAFS; High pressure; Superconductors

1. Introduction

After the discovery of high-T_c superconductor (La–Ba–Cu–O system) by Bednorz and Müller [1] in 1986, several others ceramic superconductors have been produced. Regarding ceramic superconductor families, the scientific community has shown a growing interest in relating variation of the cell parameters, oxidation state of the atoms, and other physical properties to the oxygen content or carrier doping state [2–13].

Among these several superconductor families, the mercury family $HgBa_2Ca_{n-1}Cu_nO_y$ or Hg-12$(n-1)n$ with $(n = 1, 2, 3\ldots)$ obtained by Putilin et al. [14] have shown the highest T_c (134 K). Although loss of superconductor properties due to CO_2 contamination have been observed on Hg family, this matter has been overcome by partial substitution of mercury (Hg) by rhenium (Re) [15,16]. In addition, Orlando et al. [17] have observed a clear influence of Re content on the oxygen amount present in the HgO_δ layer: Re brings additional oxygen to this site. These additional oxygen atoms are very stable and complete the mercury layer. Specifically, samples with 18% nominal atomic Re have presented an improvement of the superconducting properties [17], such as the critical current density [18], when compared with Hg-1223 ($n = 3$ without Re).

Studies concerning the influence of oxygen partial pressure used during precursor preparation and its correlation with bulk properties of $Hg_{1-x}Re_xBa_2Ca_2Cu_3O_{8+d}$

* Corresponding author. Tel.: +55 27 88130140; fax: +55 27 3352823.
E-mail address: mtdorlando@terra.com.br (M.T.D. Orlando).

0921-4534/$ - see front matter © 2005 Elsevier B.V. All rights reserved.
doi:10.1016/j.physc.2005.11.016

[(Hg,Re)-1223] polycrystalline compounds have been reported since 1999 [19–21]. These different precursor annealing treatments can modify the charge carrier number in the CuO_2 layers inside the Hg,Re-1223 superconductor. Evaluation of this charge carrier number is important to determine if the sample is over doped, optimal doped or under doped. A direct correlation between charge carrier number and the Hg-based samples produced with different annealing treatments can be obtained by thermoelectric power measurements [22,23]. Through the analysis of Hg-1223 phase diagram, a study from the under doped to over doped regions revealed a change of the thermoelectric power value at room temperature.

The charge carrier number can be correlated with the average valence of the Cu in the Cu–O layer, which, for the Hg,Re-1223 compound, depends on the Re valence in the reservoir layer. To the best of our knowledge, there are no reports in the literature about Re valence measurements. In this way, X-ray absorption spectroscopy (XAS) was used for investigating Re neighbour. In X-Ray absorption near-edge structure (XANES) the average valence state of the selected type of the atom in the sample can be obtained from the information hidden in the energy shift of the X-ray absorption edge itself [24]. The X-ray absorption near-edge spectroscopy (XANES) provides Re average valence for Re inside the (Hg,Re)-1223 as an oxygen function. Moreover, extended X-ray absorption fine structure (EXAFS) signal allows us to investigate the structural oxygen symmetry surrounding Re atom.

2. Experimental

2.1. Precursor preparation

Firstly, the standard preparation of the ceramic precursor began with a mixture of $Ba_2Ca_2Cu_3O_x$ (99.0% PRAXAIR) and ReO_2 (99.0% Aldrich) in powder form with the molar relationship of 1:0.18 [19]. These powders were homogenized in an agate mortar and compacted in a pill form with an uniaxial pressure of 0.5 GPa. The produced pellet was heated at 850 °C in a flow of oxygen (99.5%) for 15 h. The obtained precursor was crushed, homogenized and compacted again before being heated a second time at 920 °C for 12 h in a flow of oxygen. The later procedure was repeated seven more times. These thermal treatment processes are thought to provide a good homogenization of rhenium and to eliminate the carbonates remaining in the precursor sample [19,25].

2.2. Precursor annealing

The obtained precursor material was then submitted to an annealing at 920 °C for 24 h in a flowing mixture of argon (99.5% purity) and oxygen (99.5% purity) maintained at 1 bar. Three ceramic precursors have been prepared using distinct partial pressure of oxygen: 5% of O_2 and 95% of Ar (sample A), 10% of O_2 and 90% of Ar (sample B) and 15% of O_2 and 85% of Ar (sample C) [26]. One Quanta Chrome Inc. gas mixer, with controlled flow rate, was used in order to control the oxygen and the argon gas mixture proportion [20].

The XRD patterns of these sintered precursors as function of the oxygen partial pressure, P_{O_2}, are shown in Fig. 1. The X-ray diffraction measurements were carried out at Laboratório Nacional de Luz Sincroton (LNLS-Campinas-Brazil) with $\lambda = 1.54056$ Å. The identified phases were $BaCuO_{2+x}$ (101 phase), $Ba_2Cu_3O_{5+x}$ (203 phase), $Ba_4CaCu_3O_{8+x}$ (413 phase), Ca_2CuO_3, and $Ca_5Re_2O_{12}$. It can be noticed that the peaks associated with the 101 phase, which has oxygen stoichiometry variation, are slightly displaced to low angle. Thus, it indicated that there was an increase in the oxygen content of the precursor ceramics B and C, as compared with ceramic A. This interpretation is in agreement with Fujinami et al. [23]. They have achieved Hg-1223 samples with different doping state using the oxidized precursor ($BaCuO_{2+x}$). It is important to state that the displacement of the peaks have not come from the zero shift since peaks of Ca_2CuO_3 have not presented any displacement, as shown in Fig. 1.

2.3. Superconductor synthesis

Finally, the precursors prepared with different O_2 partial pressure were blended with HgO at the molar relationship of 1:0.82. They were homogenized in an agate mortar and compacted in a pellet form with an uniaxial pressure of 1 GPa. The pellets with a typical dimensions $5 \times 5 \times 20\ mm^3$ were wrapped in a gold foil (99.999%) and were introduced in a 8 mm inner diameter quartz tube. A quartz rod (7 mm diameter and 40 mm length) was also introduced together with each pellet. Each wrapped sample (A, B and C) received an extra quantity of Hg (l) which turned immediately into amalgam form with gold. The ratio between the mercury mass and the gold mass was 0.045. Based on the study of the effect of the quartz tube filling factor (ff) [27], we used $ff \cong 1.0\ g\ cm^{-3}$ and $ff_{Hg} \cong 0.010\ g\ cm^{-3}$ [20]. The quartz tubes were sealed in a high vacuum of 3×10^{-6} Torr. The average density of the pellet samples was $\rho = 4.2(2)\ g/cm^3$. All procedures have taken place inside a glove box filled with argon gas. In order to improve the grain size growth, we have also changed the annealing time to 72 h at 865 °C, as compared to Sin et al. [26]. Moreover, three sealed quartz tubes, each one with a sample inside, were put together in the same place inside an isostatic pressure furnace. The furnace was filled with 14 bar of Ar in order to avoid explosion of any quartz tube.

2.4. Sample characterization

2.4.1. X-ray diffraction and Rietveld refinement

XRD measurements were performed using laboratory diffractometers models Rigaku Multiflex and D-MAX with CuKα radiation. The spectra were measured from 2° up to

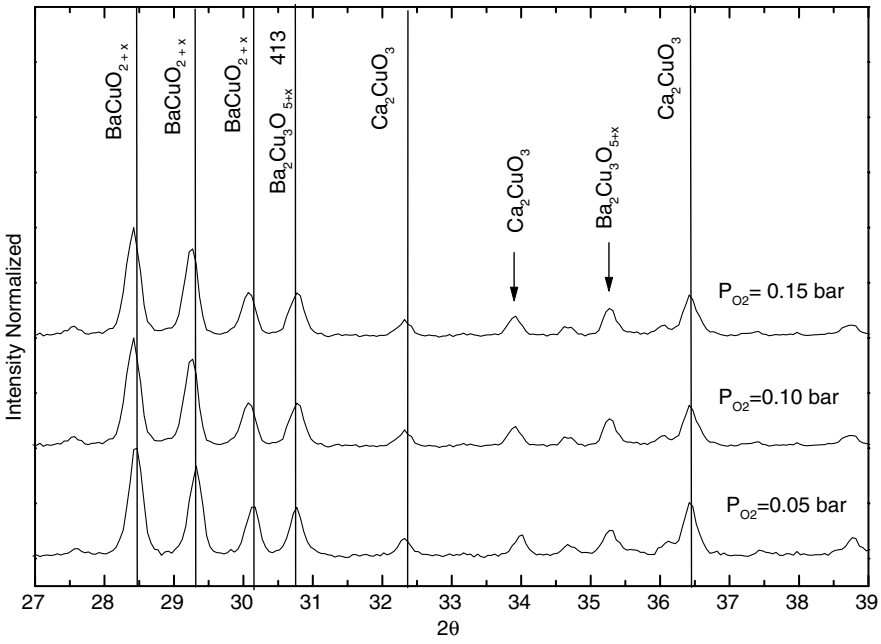

Fig. 1. XRD patterns of the precursor ceramics with different oxygen partial pressure. The identified phases were: $BaCuO_{2+x}$, $Ba_2Cu_3O_{5+x}$, $Ba_4Ca_1Cu_3O_{7+x}$, $Ca_5Re_2O_{12}$ and Ca_2CuO_3.

122° with step size of 0.01° and counting times varying from 15 to 25 s. The instrumental parameters were obtained from the refinement of standards LaB_6 and Al_2O_3 (NIST) samples. Rietveld refinements [28] were performed using the program GSAS [29] with the interface EXPGUI [30].

A typical refinement is shown in Fig. 2. The main phase found was Hg,Re-1223 (93 wt.%) residues of $HgCaO_2$, $BaCO_3$, $CaCuO_2$ and $BaCuO_2$ were also found. The phase Hg,Re-1223 was very crystalline as shown by the small broadening of their peaks. The XRD spectra of all samples were quite similar and did not show important differences

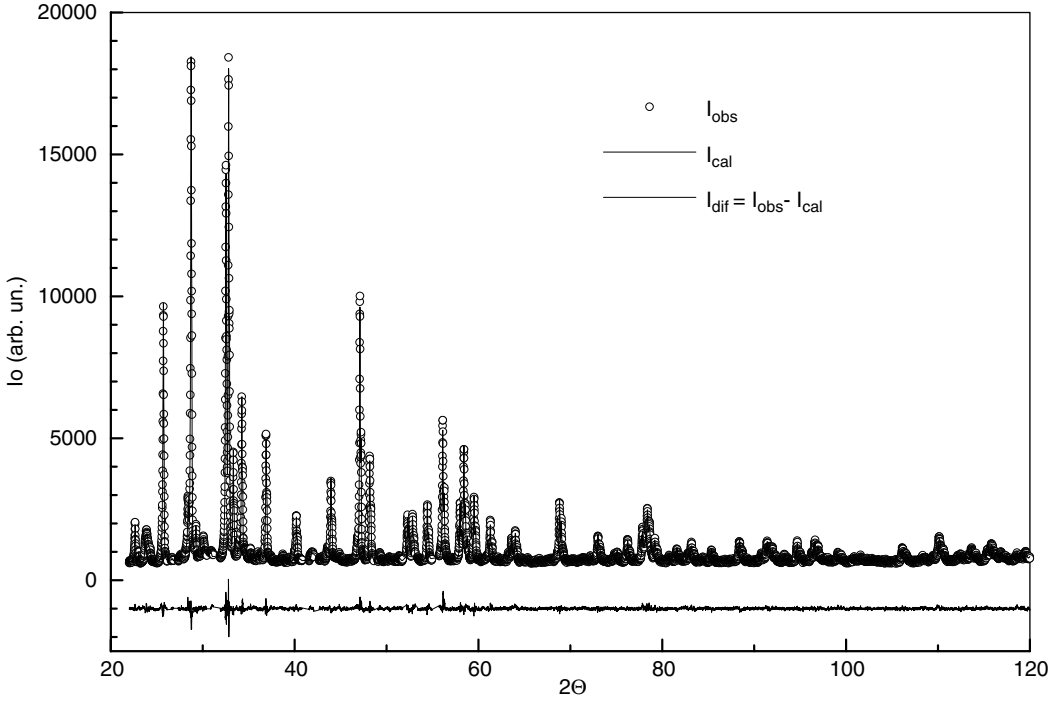

Fig. 2. Reitveld refinement of the sample B (optimal doped).

Table 1
Rietveld refinement of XRD data for samples A, B and C

	Sample		
	A	B	C
χ^2	1.942	1.837	2.195
$R(F^2)$	0.0615	0.0503	0.0514
a	3.854512(11)	3.854124(15)	3.854388(14)
c	15.687437(49)	15.688051(53)	15.689096(67)
Cu–O_{pl} angle	176.3(4)	179.8(2)	178.5(3)
DWp	1.040	1.247	0.0888
Rp	0.0346	0.0307	0.0359
Rwp	0.0441	0.0323	0.0367

in the crystal structure of the phase Hg,Re-1223. Table 1 shows the refinements results.

2.4.2. Magnetic susceptibility under hydrostatic pressure

The ac magnetic susceptibility versus temperature measurements at room pressure have exhibited closer $T_{c_{onset}}$ (A = 132.6 K, B = 133.2 K, and C = 132.7 K) for the three samples, which indicates the similar oxygen content in all samples [21]. The high-T_c cuprates superconductors have been found to show a parabolic variation of T_c as a function of the hole concentration,

$$T_c = T_c^{max} - 82.6T_c^{max}[(n - 0.160)^2], \quad (1)$$

where n is hole number per Cu–O layer [31]. Using this equation $n = 0.152$, 0.160, and 0.167 were found for A, B, and C samples respectively. Taking into account the small variation for n, similar physical properties for the three samples were expected. The ac magnetic susceptibility and ac resistivity have confirmed this assertion. However, the ac magnetic susceptibility versus temperature under external pressure have shown different $T_{c_{onset}}$ pressure dependent for each (Hg,Re)-1223 sample [21].

In order to complete Passos et al. [21] study, ac magnetic susceptibility versus temperature under different pressure range were measured: in the first pressure range, from 0 up to 1.4 GPa, a CuBe cell was used to confirm previous results [21] whereas a B4C anvill cell was required for wider pressure range, from 0.4 up to 7 GPa, in order to extend the optimal doped sample curve. Experimental details of the set up used in the first range were described in Ref. [21]. For the broader pressure range a B4C-anvil cell was built with an anvil made of B4C powder manufactured by "Hermamann Starck", with 7.9 m^2/g and pyrolitic carbon. This cell has worked at hydrostatic conditions obtained with a methanol–ethanol mixture (4:1) in a pressure cavity of 0.2 mm diameter of a CuBe gasket prepressed to 0.3 mm. The inner pressure was detected by a superconducting manometer (Pb 99.9999%, Koch-Light-Lab) placed in a gasket hole next to the sample. The primary coil (300 turns) and the astatic pair of pickup coils (2×520 turns) were produced with copper wire of 45 μm diameter. The temperature set up was the same used in Ref. [4]. Fig. 3 displays the pressure dependence of T_c. The T_c criterion was defined as the point where the χ_{ac} signal is twofold the average noise value, which was measured before superconductor transition.

In the insert of Fig. 3 it can also be observed the different dT_c/dP for samples A, B and C. Sample B presented $dT_c/dP = 1.9 \pm 0.3$ K/GPa, as a fit to a linear dependence. Sample A presented the highest value of $dT_c/dP = 8 \pm 1$ K/GPa, followed by nonlinear behaviour within 0.6–1.4 GPa pressure range. On the order hand, sample C showed negative valued of $dT_c/dP = -1.6 \pm 0.1$ K/GPa. As reported in Ref. [21], the ac magnetic susceptibility χ_{ac}

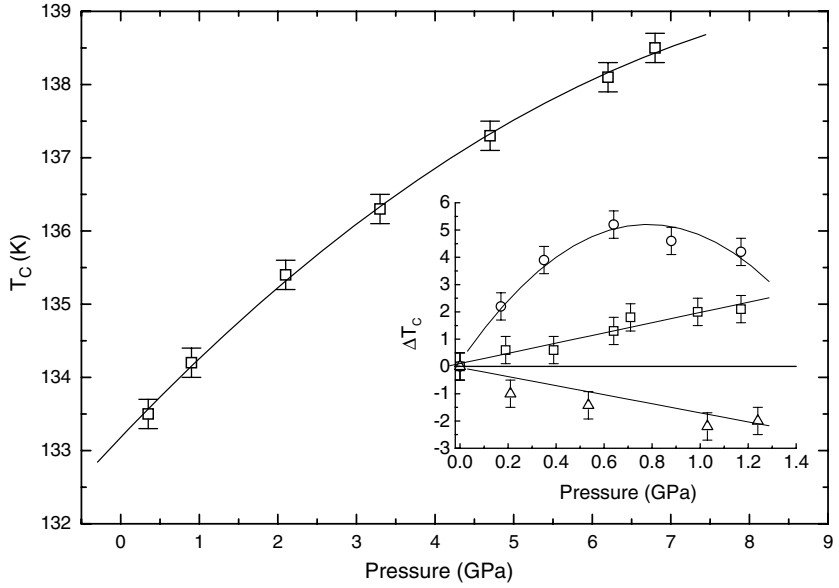

Fig. 3. T_c as a function of applied external hydrostatic pressure for sample B (optimal doped). The inset with T_c dependent of external hydrostatic pressure up to 1.4 GPa for (Hg,Re)-1223 samples prepared with different oxygen partial pressure.

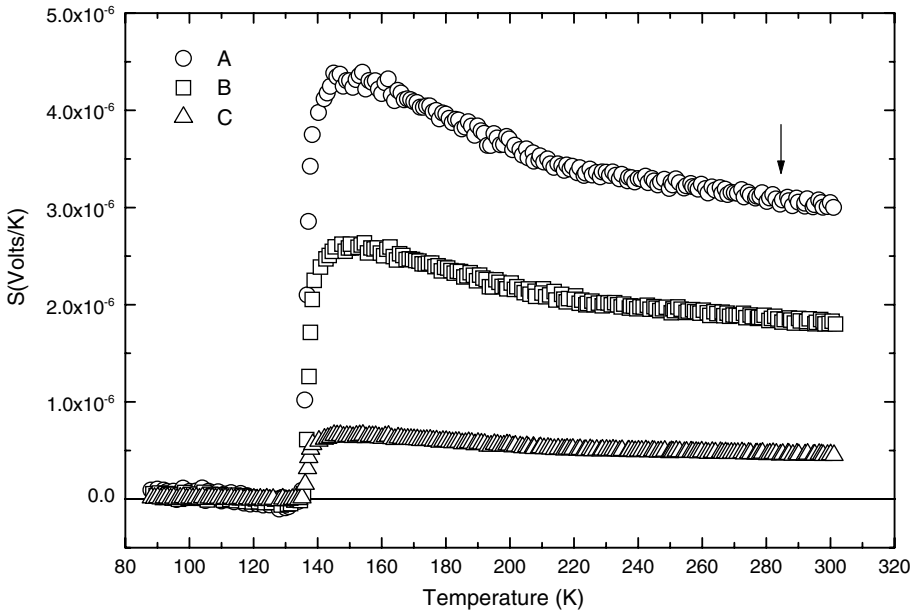

Fig. 4. Thermoelectric power of the (Hg,Re)-1223 samples with different oxygen partial pressure of the precursor annealing.

versus temperature measurements under external hydrostatic pressure can be used as a tool to confirm the doping state of $Hg_{0.82}Re_{0.18}Ba_2Ca_2$-$Cu_3O_{8+d}$ samples. Therefore, samples A, B and C were associated with the under doped, optimal doped and over doped samples, respectively.

The different T_c dependence shown in Fig. 3 may be discussed on the basis of the pressure induced charge transfer model (PICTM) modified by Almasan et al. [32]. The variation on T_c can be given by Neumeier and Zimmermann [33] equation

$$\frac{dT_c}{dP} = \frac{\partial T_c^i}{\partial P} + \left[\frac{\partial T_c}{\partial n}\right]\left[\frac{\partial n}{\partial P}\right], \quad (2)$$

where the first term is an intrinsic variation of T_c with external pressure, while the second term represents changes on T_c due to the hole concentration modified by the external pressure. For optimal doped sample the second term vanishes. Therefore, for the (Hg,Re)-1223 system $dT_c/dP = 1.9 \pm 0.3$ K/GPa correspond to the intrinsic term value found only for optimal doped sample [34].

In order to confirm the oxygen content of each sample, thermoelectric power measurements were done in the samples. The aim was to correlate the oxygen content in the precursor annealing with the charge carrier number, and, as consequence, the average hole number present in each Cu–O plane.

2.4.3. Thermoelectric power measurements

The thermoelectric power was measured on pellets with $1 \times 1 \times 7$ mm^3. Each pellet was mounted with a small heating resistance on the top and fixed on a sapphire sample holder in the bottom. The thermoelectric power measurements were carried out at constant temperature controlled by the Lake Shore Temperature 330 controller. Temperature gradients ∇T_x of the order of 0.5 K/mm were applied using a KEITHLEY 228 A power source to supply a controlled power on the small heating resistance. The ∇T_x were measured by a calibrated Au/0.07 at.% Fe–Chromel–P thermocouples made by Leico Industries Inc., and using a HP3444 digital multimeter. The voltage between the top and bottom of each sample was measured by a KEITHLEY 182 nanovoltmeter. All instrumentals were controlled and read by an IEEE-488 GPIB communication setup [35].

The results are shown in Fig. 4, and it can be observed that the thermoelectric power signal has presented a typical behaviour as described by MacIntosh and Kaiser [36]. Moreover, the thermoelectric power signal is positive and distinct at room temperature. It was shown by Obertelli et al. [37] the universal dependence of the thermoelectric power signal (at room temperature) on the hole concentration. In general, the thermoelectric power signal changes (from positive to negative) close to $n \cong 0.20$.

For $HgBa_2Ca_2Cu_3O_{8+d}$ [22] compounds, the hole concentration was found to be $n \leqslant 0.20$, which results in a positive thermoelectric power signal up to room temperature. The measurements data of the three Hg,Re-1223 samples are summarized in Table 2. The hole number per Cu–O layer n were determined by Obertelli et al. [37]

Table 2
Values of oxygen partial pressure, thermoelectric power signal at 290 K and hole number per Cu–O layer

Sample	P_{O_2} (bar)	S (μV/K)	n (hole/Cu–O)
A	0.05	3.0	0.15
B	0.10	1.8	0.16
C	0.15	0.5	0.17

universal behaviour. The values are in agreement with the hole number n from Eq. (1).

The (Hg,Re)-1223 compounds have presented a hole concentration $n < 0.20$ which is justified by the phase diagram proposed by Sin et al. [19]. When $P_{O_2} > 0.20$ oxygen partial pressure is used in the precursor annealing (over doped), the (Hg,Re)-1223 synthesis presents a segregation of (Hg,Re)-1212 and $HgCaO_2$ phases. In this case, the oxygen increment goes to the atmosphere inside the sealed quartz tube during the synthesis, as demonstrated by the TBA of the diagram $P \times T$ measurement [19]. The increase of partial pressure of oxygen, inside sealed quartz tube, shifts the equilibrium in order to form (HgRe)-1223, (Hg,Re)-1212 and $HgCaO_2$ phases. As the (Hg,Re)-1212 and $HgCaO_2$ phases are rich in oxygen, they causes a reduction of the oxygen content present in the (Hg,Re)-1223. This is the reason why a negative thermoelectric power signal in (Hg,Re)-1223 system is not found when the oxygen partial pressure was increased.

2.4.4. X-ray absorption near-edge structure measurement

Samples A, B and C were analyzed by X-ray absorption (XAS) at the XAFS station of the Laboratório Nacional de Luz Sincroton (LNLS, Campinas-Brazil), on beam line using a Si(1 1 1) double-crystal monochromator [38]. The three (Hg,Re)-1223 prepared samples as well as reference samples (ReO_2 99.9%, ReO_3 99.9%, $CaCO_3$ 99.999%, $BaCO_3$ 99.999% and HgO 99.99%) were ground to fine powder (20 μm) and then mixed with ethanol. Each mixture was vacuum decanted over a special thick (0.9 mm) paper film. The five films were mounted on the same sample holder. All spectra were taken at room temperature and they were recorded in the transmission mode using a current from 160–80 mA. The measurements of all powder were carried out at the same machine work period. The data were analyzed by the reference method with the parameters obtained from the reference powder.

In order to start the investigation about the average valence of each atoms in the $Hg_{0.82}Re_{0.18}Ba_2Ca_2Cu_3O_{8+d}$ (except copper), the samples were studied by X-ray Absorption near-edge (XANES) with step energy of 1 eV, scanning time of 1 min and 100 eV as pre-edge. The three superconductors samples were investigated using the following targets: the Re in the L_{III} edge (10.535 keV), Ba in the L_{III} edge (5.247 keV), Ca in the K edge (4.038 keV) and Hg in the L_{III} edge (12.284 keV). By XANES analysis the average valence of each element inside the (Hg,Re)-1223 compound could be determined. The results for Ba, Ca and Hg confirm the nominal valence +2 for each one (see Table 3). The rhenium (Re) valence was obtained by a fit of the energy edge shift related with each ReO_2 and ReO_3 oxides. Fig. 5 represents the measurements of XANES in the Re L_{III} edge (10.535 keV) on the five compounds (ReO_2, ReO_3, sample A, sample B and sample C). The valence of Re was assumed to be +4 and +6 in the ReO_2 and ReO_3 oxides, respectively. The energy edge values were taken at the zero of the derivate curve and correspond to abscissa of the energy edge shift versus average valence Re graphic (Fig. 5 inset). Using $E_0 = 10.535$ keV

Table 3
XANES average valence analysis

Sample	Hg	Re	Ba	Ca
A	2.0	6.8	2.0	2.0
B	2.0	6.9	2.0	2.0
C	2.0	7.0	2.0	2.0

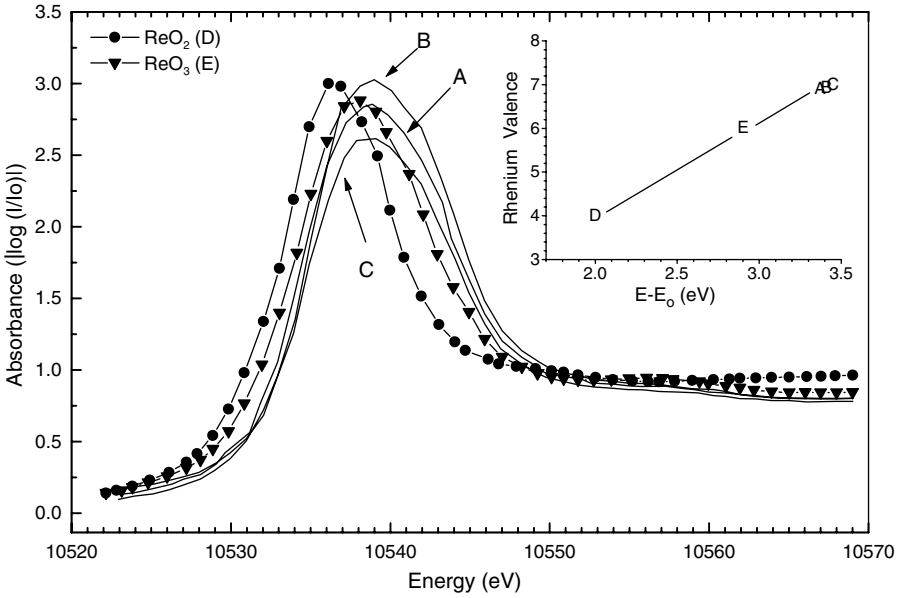

Fig. 5. The XANES spectra of all samples and the standard compounds (ReO_2 and ReO_3). The inset presents the valence curve used to determine the valence of the A, B, and C samples.

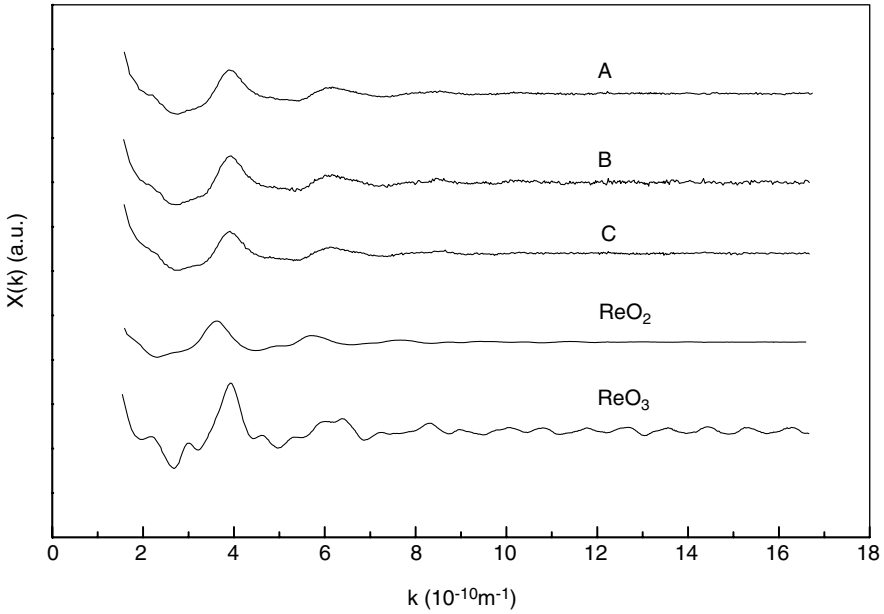

Fig. 6. The EXAFS spectra of all samples and standard compound (ReO_2 and ReO_3). There is a similar behavior as comparing A, B, C, and ReO_2 spectra.

and the ReO_2 and ReO_3 valences as reference, it was built the linear dependence of the Re valence as a function of the absorption edge shift $E - E_0$. From the line in Fig. 5 inset it was possible to extra pole the valence of rhenium (Re) for all (Hg,Re)-1223 samples. The three samples A, B and C have presented +6.8, +6.9 and +7.0 valence respectively, which is in agreement with previous valence estimated by Chmaissem et al. [12] using the Brown and Altermatt model [39].

2.4.5. Extended X-ray absorption fine structure measurement

The local Re–O octahedral oxygen coordination was investigated by extended X-ray absorption fine structure (EXAFS). The measurements were done with step energy of 1 eV, scanning time of 1 min, 100 eV as pre-edge, and 1000 eV after the edge. The three superconductors samples were investigated using the Re edge L_{III} at $E = 10.535$ keV in the transmission mode. Fig. 6 presents the EXAFS

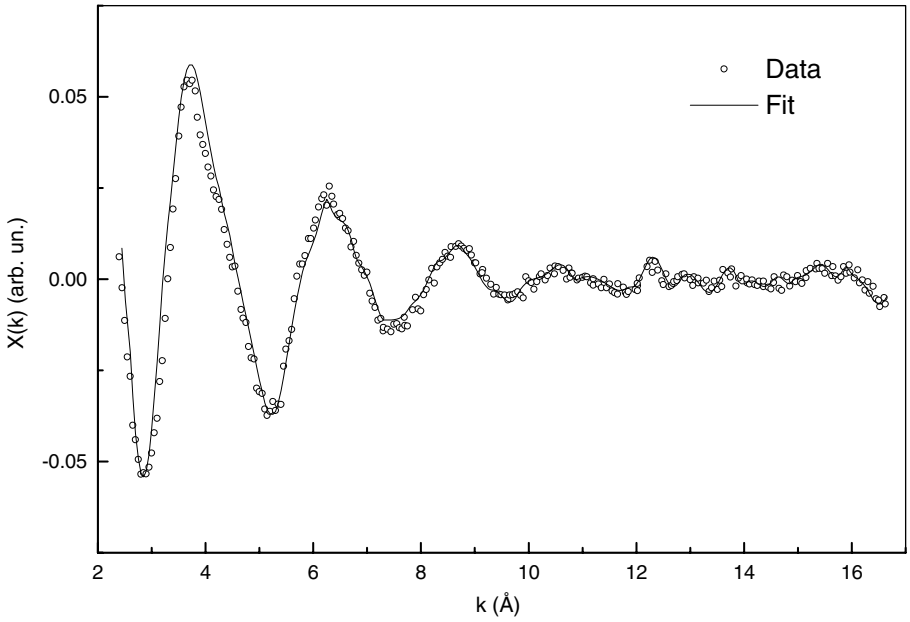

Fig. 7. The EXAFS signal of the sample B and the fit curve produced by the FEFFIT program. The initial atoms position to input the program comes from the Reitveld refinement.

Table 4
EXAFS fit parameters and Re average valence estimation [39]

	Sample		
	A	B	C
r-Factor of fit	0.008405	0.009172	0.008689
Reduced χ^2	3.190922	2.715733	2.300376
Sigma2 O_{pl} (Å^2)	0.0155 (5)	0.0137 (7)	0.0157 (8)
Dist. Re–O_{pl} (Å)	1.85 (2)	1.83 (2)	1.87 (2)
Sigma2 O_{ap} (Å^2)	0.0201 (8)	0.0165 (9)	0.0204 (6)
Dist. Re–O_{ap} (Å)	2.09 (3)	2.15 (2)	2.00 (5)
Re estimation valence	6.87	6.93	7.03

signal of A, B, C, ReO_2 and ReO_3 after 50 eV from the edge. Inspections of the A, B, and C data reveals a general signal behaviour analogous to ReO_2. Correa et al. [40] have studied X-ray powder diffraction by Rietveld refinement of the same ReO_2 (99.9%) AlfaAesar no. 62109 used here in EXAFS analysis. They have pointed out that there are two distances between Re and O in the ReO_2 (2.110 Å and 1.941 Å). In ReO_3 there is only one distance (1.875 Å) Ref. [41]. This analogous behaviour among ReO_2 and A, B, and C samples strongly suggest that the ReO_6 octahedron symmetry will present two distances also.

Data analysis of the EXAFS spectra were performed using the ATOMS, FEFF8 [42], and FEFFIT [43]. Fig. 7 shows our fit related with sample B. The fitted parameters indicated two distances in the ReO_6 octahedron introduced in superconductor *P*4/*mmm* symmetry. The first distance is Re–O_{ap} = 2.1166 Å (rhenium to apical oxygen) and the second Re–O_{pl} = 1.8247 Å (rhenium to planar oxygen). These two distances in the Brown and Altermatt model [39] give +6.93 as a valence value for the Re in Hg,Re-1223.

Complete results of the three samples are summarized in Table 4. As described before, there are two distances related with the first coordination sphere. The Re–O_{ap} distance (O_{ap} means apical oxygen) is longer than the Re–O_{pl} (O_{pl} planar oxygen) for all cases. Moreover, it can be noted that sample B has presented longer Re–O_{ap} distance than the others (A and C). By using the Brown and Altermatt [39] model it was possible to estimate the Re valence for the three cases. The results showed there exist an average valence increase of Re as oxygen content function, which are in agreement with XANES results.

3. Conclusion

The X-ray absorption near-edge spectroscopy (XANES) showed an increase of the Re oxidation state as a function of oxygen content in the three $Hg_{0.82}Re_{0.18}Ba_2Ca_2Cu_3O_{8+d}$ polycrystalline samples. The thermoelectric power measurements confirmed the smaller oxygen content increment through the carrier number present at 290 K in the three samples. The oxygen content changed the oxygen octahedral coordination surrounding Re in Hg,Re-1223. These effects were confirmed by EXAFS measurements, which revealed the ReO_6 octahedron distortion for all samples. The EXAFS signal analysis indicated that the ReO_6 octahedron introduced in the superconductor crystal symmetry is distorted with distance for Re–O_{ap} different from distance for Re–O_{pl}. Moreover, the sample produced with 10% of PO_2 has presented a shorter distance for Re–O_{pl} and a longer distance for Re–O_{ap} than the corresponding distances on the others samples (A and C). The valence evaluated by the bound length (EXAFS) in the distorted ReO_6 octahedron is in agreement with XANES analysis results (Table 4).

The distortion of the ReO_6 octahedron can be related with the T_c versus external pressure behaviour shown in the Fig. 3. In our opinion the longer Re–O_{ap} distance in sample B indicates that apical oxygen is closer to Ba and Cu in this sample than in the others samples (A and C). As consequence there exist a reduction between Cu–O_{ap} distance, which is associated to changes in the Cu–O_{pl} angle. This reduction in Cu–O_{ap} distance improves the symmetry on the CuO_4 tetrahedron. It was revealed from the Rietveld refinement (XRD) that the optimal doped sample (sample B) has presented the highest value (180°) for the Cu–O_{pl} angle (Table 1). Considering that this angle can not be changed under hydrostatic pressure, a pressure increases causes only a reduction of the distance between Cu–O_{pl} and Cu–O_{ap} without loss of symmetry in the CuO_4 tetrahedron. This scenario can justify high intrinsic value (Eq. (2)) found in the optimal doped sample under external hydrostatic pressure (Fig. 3 inset).

Acknowledgements

We would like to thank CT-Energ/CNPq Grant 504578/2004-9, CNPq 410442/2003 and CAPES. The authors are also indebted to Companhia Vale do Rio Doce and Companhia Siderúgica de Tubarão. Research performed at LNLS—National Laboratory of Light Synchrotron, Brazil (XAS #827, #1229 and #1604).

References

[1] J.G. Bednorz, K.A. Müller, Z. Phys. B 64 (1986) 189.
[2] C.W. Chu, Nature 216 (1993) 6.
[3] R.J. Wijngarden et al., Physica B 265 (1999) 168.
[4] M.T.D. Orlando et al., Phys. Rev. B 61 (2000) 15454.
[5] A. Batista-Leyva et al., Physica C 314 (1999) 73.
[6] A. Batista-Leyva et al., Physica C 383 (2003) 365.
[7] E. Altshuler et al., Physica C 371 (2002) 224.
[8] A. Bertinotte et al., Physica C 250 (1995) 213.
[9] O. Chmaissem et al., Physica C 217 (1994) 265.
[10] J.B. Torrance et al., Phys. Rev. Lett. 61 (1989) 1127.
[11] J. Shimoyama et al., Physica C 224 (1993) 1.
[12] O. Chmaissem et al., Phys. Rev. B 53 (1996) 14647.
[13] A. Sin et al., Physica C 306 (1998) 34.
[14] S.N. Putilin et al., Nature 362 (1993) 226.
[15] J. Shimoyama et al., Physica C 235–241 (1994) 2795.
[16] K. Kishio et al., J. Low Temp. Phys. 105 (1995) 1359.
[17] M.T.D. Orlando et al., Physica C 328 (1999) 257.
[18] Y. Matsumoto et al., Physica C 412–414 (2004) 435.
[19] A. Sin et al., Supercond. Sci. Technol. 12 (1999) 120.
[20] M.T.D. Orlando et al., Supercond. Sci. Technol. 13 (2000) 140.

[21] C.A.C. Passos et al., Supercond. Sci. Technol. 15 (2002) 1177.
[22] C.K. Subramaniam et al., Phys. Rev. B 51 (1995) 1330.
[23] K. Fujinami et al., Phys. Rev. B 56 (1997) 14790.
[24] I. Arcon et al., J. Am. Ceram. Soc. 81 (1) (1998) 222.
[25] S.M. Loureiro et al., Physica C 272 (1996) 94.
[26] A. Sin et al., Physica C 328 (1999) 80.
[27] A. Sin et al., Adv. Mater. 10 (1998) 1126.
[28] H.M. Rietveld, Acta Crystallogr. 22 (1967) 151.
[29] A.C. Larson, R.B. Von Dreele, General Structure Analysis System (GSAS), Los Alamos National Laboratory Report LAUR 86-748, 2004.
[30] B.H. Toby, J. Appl. Cryst. 34 (2001) 210.
[31] M.R. Pesland et al., Physica C 176 (1991) 95.
[32] C.C. Almasan et al., Phys. Rev. Lett. 69 (1992) 680.
[33] J.J. Neumeier, H.A. Zimmermann, Phys. Rev. B 47 (1993) 8383.
[34] E.L.V. Mello et al., Phys. Rev. B 56 (1997) 466.
[35] M.T.D. Orlando et al., Physica C 364–365 (2001) 350.
[36] G.C. MacIntosh, A.B. Kaiser, Phys. Rev. B 54 (1996) 12569.
[37] S.D. Obertelli et al., Phys. Rev. B 46 (1992) 14928.
[38] H. Tolentino et al., J. Synchrotron Radiat. 5 (1998) 539.
[39] I.D. Brown, D. Altermatt, Acta Cryst. B 41 (1985) 244.
[40] H.P.S. Correa et al., Braz. J. Phys. 34 (2004) 1208.
[41] J.E. Jorgensen et al., Phys. Rev. B 33 (1986) 4793.
[42] A.L. Ankudinov et al., Phys. Rev. B 58 (1998) 7565.
[43] B. Ravel et al., curse "EXAFS Analysis Using FEFF and FEFFIT"—Campinas—May 08–10, 2001, LNLS , Brazil.